The Essential Degrees of Freedom in Space-Time Fading Channels

Akbar M. Sayeed[1] and Venu Veeravalli[2]

[1] Department of Electrical and Computer Engineering
University of Wisconsin-Madison†
akbar@engr.wisc.edu

[2] Department of Electrical and Computer Engineering
University of Illinois at Urbana-Champaign
vvv@comm.csl.uiuc.edu

Abstract— **The key to reliable communication is a fundamental understanding of the interaction between the signal space and the channel. In time- and frequency-selective multi-antenna (space-time) fading channels this interaction happens in time, frequency and space. In this paper we propose a four-dimensional Karhunen-Loeve-like Fourier series representation for space-time channels that captures the essence of such interaction and exposes the intrinsic degrees of freedom in the channel. The four dimensions are: time, frequency and the two spatial dimensions at the transmitter and receiver. The key signal space parameters are the signaling duration, bandwidth and the two array apertures. The corresponding channel parameters are the delay, Doppler and the two angular spreads associated with the scattering environment. The representation induces a virtual partitioning of propagation paths in time, frequency and space that reveals their contribution to channel capacity and diversity. It also exposes fundamental dependencies between time, frequency and space thereby revealing the essential independent degrees of freedom in the channel.**

Keywords— **MIMO systems, Multipath, Doppler, Beamforming, Capacity, Diversity**

I. Introduction

The capacity and diversity afforded by a time- and frequency-selective multi-antenna (space-time) fading channel is due to the distribution of scatterers in space and the relative motion of the transmitter and receiver arrays. The distribution of scatterers and antenna array parameters determine the statistics of the space-time channel, which in turn determine the channel capacity and diversity. Accurate modeling of the scattering environment is thus paramount to realizing the full potential of antenna arrays in wireless communications. Existing channel modeling approaches completely ignore an important observation in this context: the key to reliable communication is a fundamental understanding of interaction between the channel and the signal space. An *effective channel representation* that captures the essence of such interaction is all this is needed from a communication theoretic viewpoint. In space-time channels, this interaction happens in four signal space dimensions: time, frequency, the spatial dimension at the transmitter and the spatial dimension at the receiver.

In this paper, we propose a new virtual representation for space-time channels that captures the essence of channel-signal space interaction in time, frequency and space. Each physical scatterer can be associated with a unique Angle of Departure (AoD), Angle of Arrival (AoA), delay, and Doppler shift. The virtual representation replaces the actual physical scatterers with virtual scatterers associated with fixed uniformly spaced AoD's, AoA's, delays and Doppler shifts on a four-dimensional (4D) grid. The grid spacings in the four dimensions correspond to the resolutions in time, frequency and the two spatial dimensions that are determined by the signaling bandwidth, duration, and array apertures, respectively. In essence, the virtual representation is a 4D Fourier series for the time-varying frequency response channel matrix, $\boldsymbol{H}(t,f)$, and yields many powerful insights. First, under the assumption of uncorrelated scattering, we show that $\boldsymbol{H}(t,f)$ is a segment of a 4D wide-sense stationary (WSS) process and the virtual representation coefficients constitute the corresponding uncorrelated spectral representation. Thus, the virtual representation captures the essential degrees of freedom in the channel in temporal, spectral and spatial dimensions that in turn determine its statistics, capacity and diversity. Second, via the concept of virtual scatterers, the virtual representation also yields a simple and intuitively appealing interpretation of the scattering environment and its effects on capacity [1]. Finally, the representation induces a virtual partitioning of propagation paths that explicitly reveals their contribution to channel capacity and diversity. In particular, it unravels fundamental dependencies in time, frequency and space that enables accurate estimates of channel capacity.

The next section presents a general model for space-time channels. Section III introduces the virtual representation, including the virtual path partitioning and its implications for channel statistics. Section IV discusses fundamental dependencies between time, frequency and space. Section V shows some numerical results that confirm the insights afforded by the virtual framework.

This research was supported in part by the National Science Foundation under grants CCR-9875805 and CCR-0113385, and the Office of Naval Research under grant N00014-01-1-0825.

II. A General Physical Model for Space-Time Channels

Consider a transmitter array with P elements and a receiver array with Q elements. We are interested in representing the space-time channel over a signaling duration T and two-sided bandwidth W. In the absence of noise, the transmitted and received signals are related as

$$\boldsymbol{x}(t) = \int_{-W/2}^{W/2} \boldsymbol{H}(t,f)\boldsymbol{S}(f)e^{j2\pi ft}df, \quad 0 \le t \le T, \qquad (1)$$

where $\boldsymbol{s}(t)$ is the P-dimensional transmitted signal, $\boldsymbol{S}(f)$ is the Fourier transform of the transmitted signal, $\boldsymbol{x}(t)$ is the Q-dimensional received signal, and $\boldsymbol{H}(t,f)$ denotes the *time-varying frequency response matrix* coupling the transmitter and receiver elements. We will primarily focus on $\boldsymbol{H}(t,f)$ and we index entries of $\boldsymbol{H}(t,f)$ as $H(i,k;t,f)$: $i = 0,1,\cdots,Q-1,\ k = 0,1,\cdots,P-1$.

For simplicity we focus on one-dimensional ULAs of antennas at the transmitter and receiver and consider far-field scattering characteristics. Let d_T and d_R denote the antenna spacings at the transmitter and receiver, respectively. The channel matrix can be described via the array steering and response vectors given by

$$\begin{aligned} \boldsymbol{a}_T(\theta_T) &= \frac{1}{\sqrt{P}}\left[1,\ e^{-j2\pi\theta_T},\cdots,e^{-j2\pi(P-1)\theta_T}\right]^T \\ \boldsymbol{a}_R(\theta_R) &= \frac{1}{\sqrt{Q}}\left[1,\ e^{-j2\pi\theta_R},\cdots,e^{-j2\pi(Q-1)\theta_R}\right]^T \end{aligned} \qquad (2)$$

where θ is related to the AoA/AoD variable ϕ (measured with respect to the horizontal axis — see Figure 1) as $\theta = d\sin(\phi)/\lambda = \alpha\sin(\phi)$, λ is the wavelength of propagation, and $\alpha = d/\lambda$ is the normalized antenna spacing. In this paper, we will restrict ourselves to critical $(\lambda/2)$ spacing: $\alpha_T = \alpha_R = 0.5$. In this case, there is a one-to-one mapping between $\theta \in [-0.5, 0.5]$ and $\phi \in [-\pi/2, \pi/2]$. The effect of larger antenna spacing on capacity and diversity is discussed in detail in [1].

The channel matrix $\boldsymbol{H}(t,f)$ can be generally modeled as

$$\boldsymbol{H}(t,f) = \sum_{n=1}^{N} \beta_n \boldsymbol{a}_R(\theta_{R,n})\boldsymbol{a}_T^H(\theta_{T,n})e^{j2\pi\nu_n t}e^{-j2\pi\tau_n f} \qquad (3)$$

which corresponds to signal propagation along N paths with $\{\theta_{T,n} \in [S_{T_-}, S_{T_+}] \subset [-0.5, 0.5)\}$ and $\{\theta_{R,n} \in [S_{R_-}, S_{R_+}] \subset [-0.5, 0.5)\}$ as the spatial angles (AoDs/AoAs) seen by the transmitter and receiver, respectively, $\{\nu_n = \nu(\theta_{R,n}, \theta_{T,n}) \in [-f_{\max}, f_{\max}]\}$ and $\{\tau_n = \tau(\theta_{R,n}, \theta_{T,n}) \in [0, \tau_{\mathrm{DS}}]\}$ as the Doppler shifts and delays, respectively, and $\{\beta_n\}$ as the corresponding independent complex Gaussian path gains. Note that ν_n and τ_n depend on the spatial location of scatterers, τ_{DS} denotes the delay spread and $f_{\max}$ denotes the one-sided Doppler spread. The physical model is illustrated in Figure 1(a).

III. Virtual Space-Time Channel Representation

In (3), each propagation path through the scattering environment is associated with an AoD, AoA, delay and Doppler shift which can be arbitrarily distributed within the angular, delay and Doppler spreads. The virtual representation replaces the physical propagation paths with virtual ones corresponding to fixed AoD's, AoA's, delays and Doppler shifts that are determined by the spatial, temporal and spectral resolution afforded by the finite dimensional space-time signal space. The notion of virtual angles is illustrated in Figure 1(b). The *virtual channel representation* can be expressed as

$$\begin{aligned} \boldsymbol{H}(t,f) = &\sum_{q,p,m,l} H_V(q,p;m,l)\boldsymbol{a}_R(q/Q)\boldsymbol{a}_T^H(p/P) \\ &e^{j2\pi mt/T}e^{-j2\pi lf/W} \end{aligned} \qquad (4)$$

corresponding to fixed virtual AoD's, AoA's, delays and Doppler shifts defined as

$$\tilde{\theta}_{T,p} = p/P, \quad P_- \le p \le P_+, \quad \tilde{\theta}_{R,q} = q/Q, \quad Q_- \le q \le Q_+ \qquad (5)$$

$$\tilde{\nu}_m = m/T, \quad -M \le m \le M, \quad \tilde{\tau}_l = l/W, \quad 0 \le l \le L, \qquad (6)$$

where $L = \lceil W\tau_{\mathrm{DS}} \rceil$ denotes the normalized delay spread, and $M = \lceil Tf_{\max} \rceil$ denotes the normalized Doppler spread. $P_- = \lfloor S_{T_-}P \rfloor$, $P_+ = \lceil S_{T_+}P \rceil$, $Q_- = \lfloor S_{R_-}Q \rfloor$, and $Q_+ = \lceil S_{R_+}Q \rceil$ define normalized angular spreads. The virtual channel coefficients $\{H_V(q,p;m,l)\}$ characterize the virtual representation. The spacings between the transmit/receive virtual angles represent the spatial resolutions

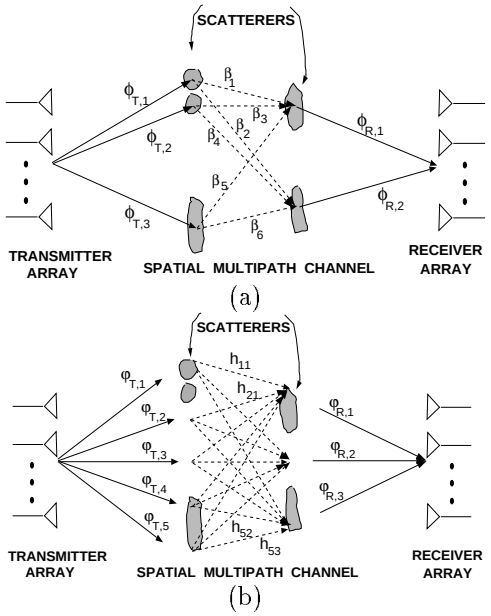

Fig. 1. *A schematic illustrating* **physical** *modeling versus* **virtual** *representation in the spatial dimension. (a)* **Physical modeling**. *Each scattering path is associated with a fading gain (β_n) and a unique pair of transmit and receive angles ($\phi_{T,n}$, $\phi_{R,n}$) corresponding to scatterers distributed within the angular spreads. (b)* **Virtual** *representation of the scattering environment depicted in (a). The virtual angles are fixed a priori and their spacing defines the spatial resolution. The channel is characterized by the virtual coefficients, $\{H_V(q,p) = h_{q,p}\}$, that couple the P virtual transmit angles, $\{\varphi_{T,p}\}$, with the Q virtual receive angles, $\{\varphi_{R,q}\}$.*

that are determined by the array apertures ($\Delta\theta_T = 1/P$ and $\Delta\theta_R = 1/Q$). The spacings between the virtual Doppler shifts and delays correspond to the spectral and temporal resolutions, respectively, and are determined by the signaling duration and bandwidth, respectively ($\Delta\nu = 1/T$ and $\Delta\tau = 1/W$).

We now address the computation of the virtual representation from $\boldsymbol{H}(t,f)$. Assume WLOG that P, Q are odd and define $\widetilde{P} = (P-1)/2$, $\widetilde{Q} = (Q-1)/2$. Note that the virtual representation (4) can be decoupled as

$$\begin{aligned}\boldsymbol{H}(t,f) &= \widetilde{\boldsymbol{A}}_R \boldsymbol{H}_V(t,f) \widetilde{\boldsymbol{A}}_T^H \quad (7)\\ \widetilde{\boldsymbol{A}}_R &= [\boldsymbol{a}_R(-\widetilde{Q}/Q), \cdots, \boldsymbol{a}_R(\widetilde{Q}/Q)] \quad (Q \times Q)\\ \widetilde{\boldsymbol{A}}_T &= [\boldsymbol{a}_T(-\widetilde{P}/P), \cdots, \boldsymbol{a}_T(\widetilde{P}/P)] \quad (P \times P), \quad (8)\end{aligned}$$

where $\widetilde{\boldsymbol{A}}_R$ and $\widetilde{\boldsymbol{A}}_T$ are discrete Fourier transform matrices, as evident from (2) and (5).[1] The matrix $\boldsymbol{H}_V(t,f)$ in (7) is the partial virtual representation with respect to space and can be computed by beamforming in the direction of virtual angles

$$\begin{aligned}\boldsymbol{H}_V(t,f) &= \widetilde{\boldsymbol{A}}_R^H \boldsymbol{H}(t,f) \widetilde{\boldsymbol{A}}_T\\ &= \sum_{l=0}^{L} \sum_{m=-M}^{M} \boldsymbol{H}_V(m,l) e^{j2\pi mt/T} e^{-j2\pi lf/W} \quad (9)\end{aligned}$$

where the second equality further decomposes $\boldsymbol{H}_V(t,f)$ into component matrices $\boldsymbol{H}_V(m,l)$ corresponding to fixed virtual Doppler shifts and delays, which can be computed from $\boldsymbol{H}_V(t,f)$ as

$$\boldsymbol{H}_V(m,l) = \frac{1}{TW} \int_0^T \int_{-W/2}^{W/2} \boldsymbol{H}_V(t,f) e^{-j2\pi mt/T} e^{j2\pi lf/W} dt\, df. \quad (10)$$

Finally, the elements of $\boldsymbol{H}_V(m,l)$ are related to the discrete physical model (3) as

$$\begin{aligned}H_V(q,p;m,l) &= \sum_n \beta_n f_Q(\theta_{R,n} - q/Q) f_P^*(\theta_{T,n} - p/P)\\ &\quad e^{-j\pi(m-\nu_n T)} \mathrm{sinc}(m - \nu_n T) \mathrm{sinc}(l - \tau_n W) \quad (11)\end{aligned}$$

were $\mathrm{sinc}(x) = \sin(\pi x)/(\pi x)$ and

$$f_Q(\theta) = \frac{1}{Q} \sum_{i=0}^{Q-1} e^{-j2\pi\theta i} = \frac{1}{Q} e^{-j2\pi\theta\widetilde{Q}} \frac{\sin(\pi Q\theta)}{\sin(\pi\theta)}. \quad (12)$$

We note that $f_Q(\theta_R)$, $f_P(\theta_T)$, $\mathrm{sinc}(T\nu)$ and $\mathrm{sinc}(W\tau)$ get peaky around the origin with increasing Q, P, T and W.

A. Virtual Path Partitioning

The virtual representation induces a partitioning of propagation paths that is very insightful in determining their contribution to capacity and diversity and to expose the dependencies between the temporal, spectral and spatial degrees of freedom in the channel. First define the following *spatial bins* in the (θ_R, θ_T) space

$$\begin{aligned}B_{T,p} &= \{(\theta_R,\theta_T) : (p-1/2)/P \le \theta_T < (p+1/2)/P\} \quad (13)\\ B_{R,q} &= \{(\theta_R,\theta_T) : (q-1/2)/Q \le \theta_R < (q+1/2)/Q\} \quad (14)\\ B_{\nu,m} &= \{(\theta_R,\theta_T) : (m-1/2)/T \le \nu(\theta) < (m+1/2)/T\} \quad (15)\\ B_{\tau,l} &= \{(\theta_R,\theta_T) : (l-1/2)/W \le \tau(\theta) < (l+1/2)/W\} \quad (16)\end{aligned}$$

corresponding to transmit spatial resolution, receive spatial resolution, spectral resolution, and temporal resolution. Define the following corresponding subsets of propagation paths

$$\begin{aligned}S_{T,p} &= \{n : \theta_{T,n} \in B_{T,p}\}, \quad S_{R,q} = \{n : \theta_{R,n} \in B_{R,q}\} \quad (17)\\ S_{\nu,m} &= \{n : \nu_n \in B_{\nu,m}\}, \quad S_{\tau,l} = \{n : \tau_n \in B_{\tau,l}\}. \quad (18)\end{aligned}$$

Note that

$$\begin{aligned}\bigcup_p S_{T,p} &= \bigcup_q S_{R,q} = \bigcup_m S_{\nu,m} = \bigcup_l S_{\tau,l}\\ &= \bigcup_{p,q,m,l} S_{T,p} \cap S_{R,q} \cap S_{\nu,m} \cap S_{\tau,l} = \{1,2,\cdots,N\} \quad (19)\end{aligned}$$

With this virtual path partitioning $\boldsymbol{H}(t,f)$ can be approximately expressed as

$$\begin{aligned}\boldsymbol{H}(t,f) &= \sum_{q,p,m,l} \left[\sum_{n \in S_{q,p,m,l}} \beta_n \right]\\ &\quad \boldsymbol{a}_R(q/Q) \boldsymbol{a}_T^H(p/P) e^{j2\pi mt/T} e^{-j2\pi lf/W} \quad (20)\end{aligned}$$

where $S_{q,p,m,l} = S_{T,p} \cap S_{R,q} \cap S_{\nu,m} \cap S_{\tau,l}$ and the virtual channel coefficients in (11) can be approximated as

$$H_V(q,p;m,l) \approx \sum_{n \in S_{q,p,m,l}} \beta_n. \quad (21)$$

The above equation states that $H_V(q,p;m,l)$ is determined by the sum of gains of all the paths whose transmit and receive angles correspond to the spatial bin

$$B_{q,p,m,l} = B_{T,p} \cap B_{R,q} \cap B_{\nu,m} \cap B_{\tau,l} \quad (22)$$

defined by the spatial, temporal and spectral resolutions in the neighborhood of the p^{th} virtual transmit angle, q^{th} virtual receive angle, m^{th} virtual Doppler shift and l^{th} virtual delay. We note that the approximations in (20) and (21) get more accurate with increasing P, Q, T and W.

B. Channel Statistics

One of the most important characteristics of the virtual representation is that the virtual coefficients $\{H_V(q,p;m,l)\}$ are approximately uncorrelated under the assumption of uncorrelated path gains: $\mathrm{E}[\beta_n \beta_{n'}^*] = \sigma_n^2 \delta_{n-n'}$ where δ_n denotes the kronecker delta function and σ_n^2 denotes the power in each path. This observation is directly evident from (21)

$$\begin{aligned}&\mathrm{E}[H_V(q,p;m,l) H_V^*(q',p';m',l')] \approx\\ &\left[\sum_{n \in S_{q,p,m,l}} \sigma_n^2 \right] \delta_{q-q'} \delta_{p-p'} \delta_{m-m'} \delta_{l-l'} \quad (23)\end{aligned}$$

[1] Note that $\widetilde{\boldsymbol{A}}_R$ and $\widetilde{\boldsymbol{A}}_T$ contain all possible virtual angles, some of which lie outside the angular spreads. $H_V(q,p;m,l)$ will be zero for those angles.

but can also be directly inferred from (11). Thus, from (20) we have

$$\begin{aligned} R_H(\Delta i, \Delta k; \Delta t, \Delta f) &= \mathrm{E}[H(i,k;t,f)H^*(i',k';t',f')] \\ &\approx \sum_{q,p,m,l} \sigma^2_{q,p,m,l} e^{-j2\pi q \Delta i/Q} e^{j2\pi p \Delta k/P} \\ &\quad e^{j2\pi m \Delta t/T} e^{-j2\pi l \Delta f/W} \end{aligned} \tag{24}$$

where $\Delta i = i - i'$, $\Delta k = k - k'$, $\Delta t = t - t'$, $\Delta f = f - f'$, and

$$\begin{aligned} \sigma^2_{q,p,m,l} &= \mathrm{E}[|H_V(q,p;m,l)|^2] \\ &= \sum_n \sigma_n^2 |f_Q(\theta_{R,n} - q/Q)|^2 |f_P(\theta_{T,n} - p/P)|^2 \\ &\quad |\mathrm{sinc}(m - \nu_n T)|^2 |\mathrm{sinc}(l - W\tau_n)|^2 \qquad (25) \\ &\approx \sum_{n \in S_{q,p,m,l}} \sigma_n^2 \qquad (26) \end{aligned}$$

is the power in the virtual coefficient $H_V(q,p;m,l)$ and the approximation in (26) corresponds to virtual path partitioning. Relation (24) yields the insightful conclusion that under the assumption of uncorrelated path gains, $\boldsymbol{H}(t,f)$ is a segment of a 4D WSS process in the two spatial dimensions, time and frequency, and the virtual coefficients $\{H_V(q,p;m,l)\}$ are the corresponding uncorrelated spectral representation. Furthermore, (26) states that the power in $H_V(q,p;m,l)$ is equal to the sum of the powers in the paths that lie in the spatial bin $B_{q,p,m,l}$ defined in (22).

IV. Fundamental Dependencies in Time, Frequency and Space

From (4) we may conclude that the total independent degrees of freedom in the space-time channel are

$$N_{ST} = (Q_+ - Q_- + 1)(P_+ - P_- + 1)(L+1)(2M+1) = N_S N_T \tag{27}$$

where $N_S = (Q_+ - Q_- + 1)(P_+ - P_- + 1)$ represents the degrees of freedom in space and $N_T = (L+1)(2M+1)$ represents the degrees in time (and frequency). However, this conclusion implicitly assumes that the degrees of freedom in space, time and frequency are independent. Thus (27) serves as an upperbound and we now use the notion of virtual path partitioning to demonstrate that there are fundamental dependencies between time, frequency and space and thus the essential degrees of freedom in the channel may be less than the upperbound in (27).

The fundamental dependencies between time, frequency and space are due to the fact that the delay and Doppler spreads are related to the angular spreads — larger angular spreads result in larger delay and Doppler spreads. For given (q,p), $H_V(q,p;m,l)$ is non-vanishing over (m,l) for $l = L_{-(q,p)}, \cdots, L_{+(q,p)}$ and $m = M_{-(q,p)}, \cdots, M_{+(q,p)}$ where

$$L_{-(q,p)} = \left\lfloor \left[\min_{B_{q,p}} \tau(\theta) \right] W \right\rfloor, \quad L_{+(q,p)} = \left\lceil \left[\max_{B_{q,p}} \tau(\theta) \right] W \right\rceil \tag{28}$$

$$M_{-(q,p)} = \left\lfloor \left[\min_{B_{q,p}} \nu(\theta) \right] T \right\rfloor, \quad M_{+(q,p)} = \left\lceil \left[\max_{B_{q,p}} \nu(\theta) \right] T \right\rceil \tag{29}$$

Consequently, the virtual representation (4) can be refined to limit the ranges of l and m as a function of (q,p) as above to reflect the truly essential (independent) degrees of freedom in the channel

$$N_{ST,ess} = \sum_{q,p} \sum_{l=L_{-(q,p)}}^{L_{+(q,p)}} \sum_{m=M_{-(q,p)}}^{M_{+(q,p)}} \leq N_{ST}. \tag{30}$$

Note that $N_{ST,ess} = N_{ST}$ in (27) if and only if $(L_+ - L_- + 1)(M_+ - M_- + 1) = (L+1)(2M+1)$ for all (q,p) which would seldom be true particularly for channels that are *underspread* ($\tau_{\mathrm{DS}} f_{\max} \ll 1$) in time and frequency. This is because time- and frequency-selectivity exhibited by $H_V(q,p;t,f)$ depends on the spatial resolution of the array: higher resolutions would result in less selectivity whereas lower resolutions will result in higher selectivity. In particular, a SISO channel will exhibit maximum time and frequency selectivity. For larger number of antennas, the degrees of freedom in time and frequency are distributed between the spatial channels defined by different pairs of virtual transmit and receive angles.

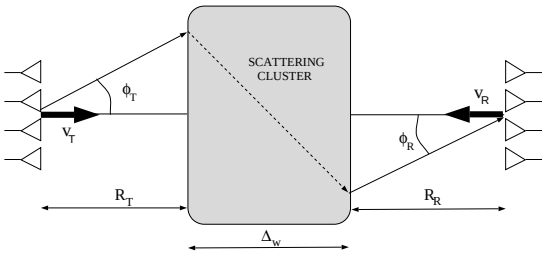

Fig. 2. *A schematic illustrating the dependence of delay and Doppler shift on the virtual transmit and receive angles.*

To quantify dependencies between time, frequency and space we have to specify explicit dependence of ν and τ on (θ_R, θ_T). Figure 2 illustrates a simple scattering geometry to quantify such dependencies. Consider a single scattering cluster at a distance R_T from the transmitter and R_R from the receiver. Suppose that v_T denotes the relative velocity between the transmitter array and the cluster and v_R denotes the relative velocity between the receiver array and the cluster. Let Δ_T and Δ_R denote the angular spreads seen by the transmitter and receiver, and Δ_w denote the "width" or "depth" of the scattering cluster. Via simple geometric considerations depicted in Figure 2, $\tau(\theta_R, \theta_T)$ and $\nu(\theta_R, \theta_T)$ can be estimated for any given (θ_R, θ_T) as

$$\tau(\theta) = \sqrt{\Delta_w^2 + |R_T\theta_T/\alpha_T - R_R\theta_R/\alpha_R|^2}/c \tag{31}$$

$$\nu(\theta) = f_{\max,\mathrm{T}} \sqrt{1 - {\theta_T}^2/\alpha_T^2} + f_{\max,\mathrm{R}} \sqrt{1 - {\theta_R}^2/\alpha_R^2} \tag{32}$$

where c denotes the speed of light, $f_{\max,\mathrm{T}} = v_T/c$ and $f_{\max,\mathrm{R}} = v_R/c$ (which could be positive or negative depending on the direction of relative motion). From (31) and (32) we see that ν depends on the relative velocities and the angular spreads, whereas τ depends on the angular spreads as well as the "width" of the cluster. We note the expression for τ is stricly a lowerbound since intermediate scattering within the cluster may result in longer delays.

V. Numerical Results

We now present some numerical results to illustrate the effect of time/frequency selectivity on capacity and the effect of number of antennas on time/frequency selectivity of the channel.

We simulated a single scattering cluster, as in Figure 2, with angular spreads of $\Delta_T = \Delta_R = 2\pi/3$ centered at $(\phi_T, \phi_R) = (0, 0)$. We considered $N = 100$ propagation paths. We first generated N pairs of angles, $\{\phi_{R,n}, \phi_{T,n}\}$, uniformly distributed, within the angular spreads to fix the scatterer positions. To simulate time/frequency selectivity, we considered a temporal signal space with $N_o = TW = 65$ dimensions. We simulated three types of channels. **CH 1** (flat): $R_T = R_R = 1000$m, $f_{\max,\mathrm{R}} = f_{\max,\mathrm{T}} = 50$ Hz, $W = 1$ MHz, $T = 65\mu s$. **CH 2** (medium selective): $R = 8000$m, $f_{\max} = 400$ Hz, $W = 1$ MHz, $T = 65\mu s$. **CH 3** (highly selective): $R = 8000$m, $f_{\max} = 400$ Hz, $W = 10$ MHz, $T = 6.5\mu s$. $\Delta w = 100$m in all cases. Note that **CH 1** and **CH 2** have the same T and W but **CH 2** corresponds to larger delay and Doppler spreads and thus is more selective. **CH 3** has the same delay and Doppler spread parameters but is even more selective than **CH 2** due to its higher bandwidth (delay diversity is easier to exploit in this set up). Realizations of the three channels were generated using (3) by simulating the fading gains as iid complex Gaussian random variables. Each realization was normalized to yield $\sum \beta_n^2 = PQ$.

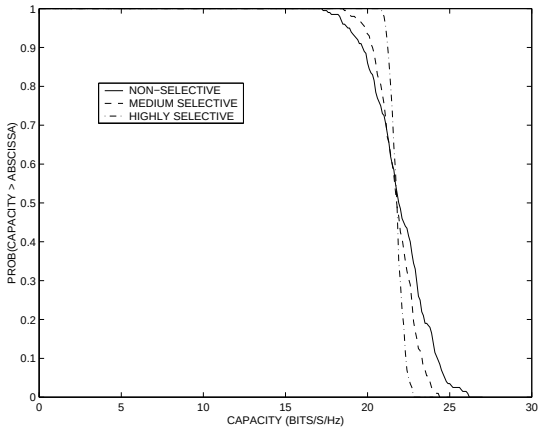

Fig. 3. *Comparison of the three channels illustrating the effect of time/frequency selectivity on outage capacity.*

Figure 3 illustrates the effect of time/frequency selectivity on outage capacity for $P = Q = 4$ antennas. The capacity was numerically computed using 200 independent channel realizations at an SNR of 20dB (details to be reported elsewhere due to lack of space). As evident, the outage capacity curves get steeper (higher diversity) as the channel gets more selective. The ergodic capacity of all three channels is approximately 21.8 bits/s/Hz. Note that this is consistent with the experimental results recently reported in [2] and in disagreement with analytical results reported in [3] which suggested that increased delay spread can increase ergodic capacity. Our framework strongly suggests that this conclusion is incorrect and is based on the channel modeling assumptions used in [3] (details to be reported elsewhere).

Figure 4 illustrates the dependencies between time, frequency and space. **CH 2** was simulated using $P = Q = 2$ and $P = Q = 4$ antennas. The figure shows the contour plots of the power in non-vanishing virtual delay-Doppler coefficients, $\sigma^2_{q,p,m,l}$, for a representative (q, p) in the two cases. It is evident that the delay-Doppler spread decreases in the virtual spatial domain for larger number of antennas, as predicted by our analysis. Note that the number of significant $\sigma^2_{q,p,m,l}$ provides an estimate for $N_{ST,eff}$ in (30). Our simulations yielded $N_{ST,eff}/QP = 4.5$ in the 2-antenna channel and 2.75 in the 4-antenna channel, confirming that the delay-Doppler diversity (time/frequency selectivity) decreases with increasing number of antennas.

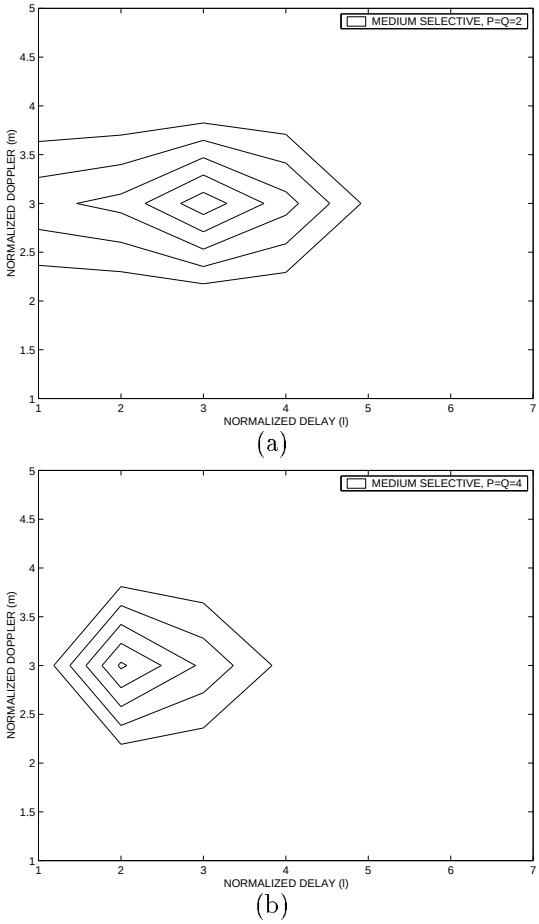

Fig. 4. *Contour plots of the powers in a subset of non-vanishing virtual delay-Doppler coefficients for* **CH 2** *for a representative virtual angle pair* (q, p). *(a)* $Q = P = 2$. *(b)* $P = Q = 4$.

References

[1] A. M. Sayeed, "Deconstructing multi-antenna fading channels," *to appear in the IEEE Trans. Signal Processing*, 2002.

[2] A. F. Molisch, M. Steinbauer, M. Toeltsch, E. Bonek, and R. S. Thomä, "Capacity of MIMO systems based on measured wireless channels," *IEEE J. Selec. Areas. Commun.*, vol. 20, pp. 561–569, Apr. 2002.

[3] H. Bolcskei, D. Gesbert, and A. J. Paulraj, "On the capacity of OFDM-based spatial multiplexing systems," *IEEE Tran. Commun.*, vol. 50, pp. 225–234, Feb. 2002.